analytical chemistry

Article

Cite This: Anal. Chem. 2017, 89, 11098-11106

pubs.acs.org/ac

Development of Visible-Light Induced Photoelectrochemical Platform Based on Cyclometalated Iridium(III) Complex for Bioanalysis

Chunxiang Li,[†,‡] Weisen Lu,[‡] Ming Zhu,[‡] and Bo Tang*[,†]

[†]College of Chemistry, Chemical Engineering and Materials Science, Collaborative Innovation Center of Functionalized Probes for Chemical Imaging in Universities of Shandong, Key Laboratory of Molecular and Nano Probes, Ministry of Education, Institute of Molecular and Nano Science, Shandong Normal University, Jinan 250014, P. R. China

[‡]Key Laboratory of Sensor Analysis of Tumor Marker Ministry of Education, College of Chemistry and Molecular Engineering, Qingdao University of Science and Technology, Qingdao 266042, P. R. China

Supporting Information

ABSTRACT: The performance of the photoelectrochemical (PEC) bioanalysis relies closely on the properties of the used photoactive species. In this study, a visible-light induced PEC active species, $[(C6)_2Ir(dcbpy)]^+PF_6^-$ (C6 = coumarin 6, dcbpy = 2,2′-bipyridine-4,4′-dicarboxylic acid) was prepared based on C6 with the stronger absorbance in the visible region. The as-prepared complex was characterized by ^1H NMR, UV−visible absorption and cyclic voltammetry. It exhibits intense absorption in visible region at 480 nm with a molar extinction coefficient (ε) of more 40000 M^{-1} cm^{-1}, which is approximately twice that of $Ru(bpy)_3^{2+}$. The PEC behaviors of the iridium(III) complex were investigated through covalently attaching to the ITO electrode. Induced by visible light, a large and stable cathodic photocurrent can be observed when dissolved O_2 is served as a sacrificial electron acceptor. Also probable mechanisms of photocurrent generation are deduced. Employing $[(C6)_2Ir(dcbpy)]^+PF_6^-$ as signal reporter, the Au NPs-based nanoprobe was constructed and successfully applied to assembly PEC platform based on the Exo III-assisted recycling amplification for bioanalysis. With thrombin as a model analyte, the PEC platform was found to be logarithmically proportional to thrombin concentrations across the range from 20 fM to 10 pM with fine selectivity, indicating excellent PEC properties of the synthesized Ir(III) complex and enormous potential for PEC bioanalysis.

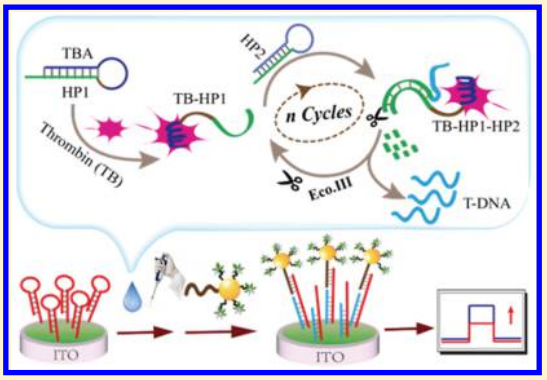

Photoelectrochemical (PEC) analytical technique has revealed its tremendous potential for biological assays.[1−3] PEC process is exactly the reverse of electrochemiluminescence (ECL), which employing light as input and the transduced electrical signal as the detection readout. Benefiting from total separation of excitation and detection, the technique has higher sensitivity than traditional electrochemical and optical means because of the lower background signals. While it inherits electrochemical advantages, such as low cost, simple instrument, and easy miniaturization. Undoubtedly, the analytical performance of the PEC system, especially the detection sensitivity, depends intimately on the utilized photoactive species. Although numerous semiconducting nanoparticles or quantum dots, CdS, CdSe in most cases, have been investigated for PEC study toward various analytes,[4−8] they suffered from the high toxicity of cadmium and poor reproducibility of nanomaterials.[9] As an important branch, metal−organic complexes are known to be a remarkable species for PEC application because of their high thermal stability, appropriate redox and photophysical characters. To date, most of the PEC studies on metal−organic complexes merely focused on Ru(II) complexes, and $Ru(bpy)_3^{2+}$ and its derivatives-based PEC system have been extensively applied to detect DNA and immunoassay.[10−13] The success of Ru(II) complexes as photoactive species for EC bioanalysis stimulates the search for other metal-based complexes.

As typical metal−organic complexes, cyclometalated Ir(III) complexes have attracted a lot of attention over the past decades due to their enormous potential application in optoelectronic devices, such as organic light-emitting devices (OLEDs),[14,15] organic photovoltaics (OPVs),[16−18] photo-induced hydrogen (H_2) generation,[19,20] and dye-sensitized solar cells (DSSCs).[21,22] These diverse applications originates from the unique triplet state properties of Ir(III) complexes, including the long excited state lifetimes, the tunable triplet-state energies and redox potentials.[23] Despite the rapid development, exploiting iridium(III) complex as photoactive species for PEC bioanalysis is just starting. Recent prominent reports from Cosnier et al. verified that a new cyclometalated

Received: August 10, 2017
Accepted: September 21, 2017
Published: September 21, 2017

DOI: 10.1021/acs.analchem.7b03229
Anal. Chem. 2017, 89, 11098−11106

Ir(III) complex bearing pyrrole groups showed similar PEC performances and comparable photocurrent efficiency to $Ru(bpy)_3^{2+}$ complex through electropolymerization at electrodes.[24] More recently, our group designed and synthesized a photoactive intercalators $[(ppy)_2Ir(dppz)]^+PF_6^-$ and use it to successfully establish an effective PEC sensing platform for sensitive determination of target DNA.[25] These results were promising and motivate to further exploit of novel Ir(III) complexes for PEC applications. In particular, Ir(III) complexes show advantageous excited-state natures over Ru(II) complexes. Except triplet metal-to-ligand charge transfer (^{3}MLCT), triplet ligand-to-ligand charge transfer (^{3}LLCT) and triplet state of intraligand (^{3}IL) were also involved.[26] And most remarkably, their photophysical and electrochemical properties are tunable over a broad range in a predictable way, indicating significant potential for achieving novel PEC applications.

However, weak visible absorption natures of traditional cyclometalated Ir(III) complexes limited further application for PEC system due to low photocurrent conversion efficiency. To achieve strong absorption in the visible range, an effectual approach is to affiliate a visible light-harvesting chromophore to the coordinated center. For example, the Ir(III) complexes with boron dipyrromethene (Bodipy) showed strong visible absorption and were used as triplet photosensitizers for TTA upconversion.[27] Coumarin 6 (C6) is a common fluorescent laser dye, which possesses the required structures allowing them to coordinate with Ir(III) metal center. And the obtained complex $(C6)_2Ir$ (acac), acac = acetyl acetone) was endowed strong visible absorption ($\varepsilon \approx 50000\ M^{-1}\ cm^{-1}$).[28] Murata's group reported cationic iridium(III) complexes with C6 as cyclometalated ligand exhibits a high ε value of 129 000 $M^{-1}\ cm^{-1}$ at 483 nm, which was used as sensitizer for visible-light-driven H_2 generation.[29] Also, the Elliot's group investigated the use of visible-light-absorbing complex base on C6 as a sensitizer in DSSCs.[30] Integrating strong visible-light-absorbing with the advantages of cyclometalated iridium(III), we tentatively undertake a pilot study to apply this type of complexes in PEC system to achieve a series of novel photoactive materials with improved and stable photocurrent. Thus, in this study, a cationic iridium(III) complex, $[(C6)_2Ir(dcbpy)]^+PF_6^-$ (dcbpy = 2,2′-bipyridine-4,4′-dicarboxylic acid) was prepared, employing C6 as cyclometalated ligand and 2,2′-bipyridine with pendent carboxyl groups as an auxiliary ligand to allow for the convenient covalent attachment (Scheme 1). The UV−vis absorption, electrochemical, and PEC characters of the Ir(III) complex were studied. Adopting $[(C6)_2Ir(dcbpy)]^+PF_6^-$ as signal reporter, the Au NPs-based nanoprobe was constructed and successfully applied to assembly PEC bioanalysis platform based on the Exo III-assisted recycling amplification. To our knowledge, it is the first example that visible-light induced Ir(III) complex-based PEC platform was fabricated. We look forward that this precursor work will be valuable for exploiting admirable Ir(III) complexes as photoactive species for PEC bioanalysis.

Scheme 1. Molecular Structure of $[(C6)_2Ir(dcbpy)]^+PF_6^-$

EXPERIMENTAL SECTION

Materials and Reagents. Indium tin oxide (ITO) slices coating 185 ± 5 nm, sheet resistance 6−8 Ω/square) were purchased from Xiang Science & Technology (China). (3-Aminopropyl) triethoxysilane (APTES), triethanolamine (TEOA), ascorbic acid (AA), hydrogen peroxide (H_2O_2) (30%), and ammonium hydroxide (NH_4OH) (30%) were obtained from Aladdin. Tris(2-carboxyethyl) phosphine hydrochloride (TCEP), 1-ethyl-3-(3-dimethylaminopropyl) carbodiimide (EDC), cysteamine, *N*-hydroxysuccinimide (NHS), human thrombin, and trypsin were from Sigma-Aldrich. Tetrabutyl ammonium hexafluorophosphate (Bu_4NPF_6) was obtained from JK (China). Exo III was from New England Biolabs Ltd. Human IgG and Bovineserum albumin (BSA) and all the oligonucleotides in this work were supplied by Sangon Biological Engineering Technology Co., Ltd. (Shanghai, China). The oligonucleotide sequences involved (from 5′−3′) are as follows: HP1, CCA CAC CAA CCT CTT CGT TTC TTG GTT GGT GTG GTT GG; HP2, CAA CCT CTT CGT AGA GAG GTG TTT CCG AAG AGG TTG GTG TGG; HP3, CTT CGT AGA GAG GTG CAC GAT TTC CAC CTC TCT ACG AAG AGG TTG-SH; Probe DNA, CAC CTC TCT ACG AAG TT-$(CH_2)_6$-SH.

All oligonucleotides stock solutions were prepared through diluting with 10 mM Tris-HCl buffer (50 mM NaCl, 10 mM $MgCl_2$, pH 7.9). Boracic acid buffer (0.1 M, pH = 9.0) was prepared by mixing the stock solutions of H_3BO_3 and $Na_2B_4O_7$. All hairpin oligonucleotides were pretreated with a procedure of heat incubation at 90 °C for 2 min and then slowly cooled down to room temperature.

Apparatus. ^{1}H NMR spectra were obtained employing a Bruker AV 500 MHz spectrometer. Cyclic voltammetry (CV) were measured in dry CH_3CN with Bu_4NPF_6 (0.1 M) as the supporting electrolyte on an electrochemical workstation (CHI 660D). Glassy carbon disk (2 mm), platinum wire, and saturated Ag/AgCl were served as working electrode, counter electrode, and reference electrode, respectively. The UV−vis spectra were obtained in a Shimadzu UV-2600 spectrometer. Electrochemical impedance spectroscopy (EIS) was recorded on an electrochemical workstation (CHI 660D) with a three-electrode system in PBS (0.1 M, pH = 7.4) containing 10 mM $Fe(CN_6)^{3-/4-}$ (1:1) mixture as the redox probe in the frequency range of 0.1 Hz−100 kHz under an amplitude of 5 mV. PEC assays were carried out with MPI-EO PEC analysis system (Xi'an Remex Analysis Instrument Co., Ltd., Xi'an, China). A Xe lamp (150 W) assembled with monochromator (omni-λ 150, Zolix) was used as the excitation light source. A modified ITO electrode with fixed area (0.25 cm^2), platinum wire, and saturated Ag/AgCl were served as working electrode, counter electrode, and reference electrode, respectively.

Synthesis of the Ligand C6 and the Complex $[(C6)_2Ir(dcbpy)]^+PF_6^-$. The ligand C6 and the complex $[(C6)_2Ir(dcbpy)]^+PF_6^-$-NHS were prepared according to the reported methods with proper modifications (see the Supporting Information).[31−33]

Preparation of $[(C6)_2Ir(dcbpy)]^+PF_6^-$ Modified ITO Electrode. ITO electrode surface was cleaned successively using acetone, ethanol, and ultrapure water by ultrasonic treatment for 15 min and then dried under N_2 atmosphere at

DOI: 10.1021/acs.analchem.7b03229
Anal. Chem. 2017, 89, 11098−11106

room temperature. The clean ITO electrode was immersed in a mixture solution of H_2O, NH_4OH and H_2O_2 (5:1:1, V/V/V) for 1 h to form monolayer of hydroxyl on the surface of the ITO electrode. Then, the electrode was rinsed with ultrapure water and dried under N_2 atmosphere. Then ITO electrode was dipped into APTES solution in ethanol (5%) for 12 h to form NH_2-rich self-assembled layer. After thorough rinsing with ethanol, the ITO slice was heated to 80 °C to remove nonspecifically adsorbed APTES. The modified ITO was immersed in the 0.1 mM $[(C6)_2Ir(dcbpy)]^+PF_6^-$-NHS solution in boracic acid buffer (0.1 M, pH = 9.0) for 2 h. The photocurrent intensities of the thus-obtained electrodes were measured in 0.1 M PBS solution (pH = 7.4).

Preparation of AuNPs Nanoprobes. AuNPs were prepared on the basis of previous method with appropriate modification and the procedure was presented in the Supporting Information.[34] AuNPs-based nanoprobe was constructed according to the method reported previously.[35] TCEP (6 μL,10 mM), P-DNA (7.2 μL, 100 μM), and cysteamine (7.2 μL, 100 μM) were mixed and reacted for 30 min at room temperature to activate SH. Then the above-prepared AuNPs (1 mL) was added to the mixture and incubate for 6 h at ambient temperature. Subsequently, $[(C6)_2Ir(dcbpy)]^+PF_6^-$–NHS solution (150 μL,0.5 mM) in boracic acid buffer (0.1 M, pH 9.0) was added, and the resulting mixture reacted with gentle shaking for 12 h. Then the solution was centrifuged at 12000 rpm for 20 min and resuspended in 800 μL of washing boracic acid buffer, repeat 3 times. Finally, the synthesized AuNPs nanoprobe was dispersed to 10 mM Tris-HCl buffer and was stored at 4 °C for the following assay.

Exo III-Assisted Recycling Assay. The mixture (50 μL) containing HP1 (0.2 μM), HP2 (0.2 μM), Exo III (20 units), and different concentrations of thrombin in 10 mM Tris-HCl buffer (50 mM NaCl, 10 mM $MgCl_2$, pH 7.9) was incubated for 1.5 h at 37 °C. Then the solution was heated at 80 °C for 10 min to deactivate Exo III and prevent the digestion reaction. The obtained solution was used for the following fabrication process of ITO electrode.

Fabrication of ITO Electrode. The washing of the ITO electrode and the process of modification with AuNPs were performed according to the same method as above. The hairpin DNA HP3 was diluted in 10 mM Tris-HCl buffer (50 mM NaCl, 10 mM $MgCl_2$, 10 mM TCEP, pH 7.9) and reacted for 1 h to split disulfide bonds. Then 20 μL of HP3 solution (1 μM) was dropped onto the surface of ITO slice modified with AuNPs at 37 °C for 12 h to obtain the AuNPs/HP3 electrode. The AuNPs/HP3 electrode was then dipped into 2 mM MCH solution in Tris-HCl buffer (10 mM) for 1 h to block the uncovered electrode surface to get AuNPs/HP3/MCH electrode. After that, 20 μL of the above target recycling mixture was dropped onto the electrode surface of AuNPs/HP3/MCH and kept at 37 °C for 2 h to capture the released T-DNA. Finally, 20 μL of the above AuNPs nanoprobes was dropped onto the surface of the assembled electrode for further hybridization at 37 °C for 2 h. Thus, the PEC signal probes were loaded. The ITO electrode was rinsed three times with Tris-HCl buffer (10 mM) after each assembly step.

Photoelectrochemical Measurement. The photocurrent intensity of the working electrode was measured in PBS solution (0.1 M, pH = 7.4) illuminated by 475 nm light containing 0.1 M AA as sacrificial electron donor. The light was switched on and off every 20 s, and the applied potential was 0 V.

Real Samples Analysis. Human serum were kindly supplied by Qingdao Central Hospital and stored at 4 °C. The human serum from healthy volunteers was 20-fold diluted with 10 mM Tris–HCl buffer (50 mM NaCl, 10 mM $MgCl_2$, pH 7.9). Three various concentrations of thrombin, 50, 500, and 5000 fM, was added into the diluted human serum, respectively. Working electrode assembly and PEC measurement methods were the same as that for the detection of thrombin standards.

RESULTS AND DISCUSSION

UV–vis Absorption and Electrochemical Properties. The UV–vis spectrum of $[(C6)_2Ir(dcbpy)]^+PF_6^-$ in CH_3CN are presented in Figure 1. Unlike conventional phenyl pyridine-based Ir(III) complex,[36,37] the absorption of $[(C6)_2Ir(dcbpy)]^+$ is characterized by very intense coumarin 6-based absorbance in the visible region at 480 nm with a shoulder (ε = 42000 M^{-1} cm^{-1}), which is assigned to ILCT of C6. It is notable that the ε value of this Ir(III) complex is approximately twice that of $Ru(bpy)_3^{2+}$ at 450 nm (ε = 22000 M^{-1} cm^{-1}) and bathochromically shifted by over 30 nm (Figure 1). Such strong visible absorption indicates the potential for efficient photoelectric conversion material. The Ir(III) complex showed absorption bands at 230, 255, and 310 nm, which were attributed to spin-allowed ligand-centered intraligand ($\pi \rightarrow \pi^*$) transitions from dcbpy. The E_{0-0} energy was estimated to be 2.25 eV based on the onset absorption spectrum according to $E_{0-0} = 1240/\lambda_{onset}$.

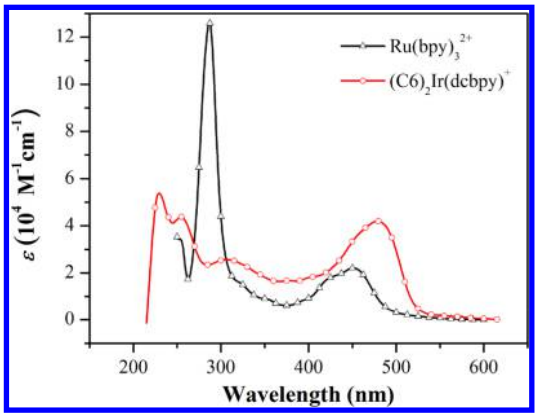

Figure 1. Absorption spectra of $[(C6)_2Ir(dcbpy)]^+PF_6^-$ and $Ru(bpy)_3^{2+}$ (1.0×10^{-5} M) in CH_3CN.

The redox nature of the complex was inspected by cyclic voltammetry. Measurement was carried out in deoxygenated anhydrous CH_3CN containing 0.1 M Bu_4NPF_6 as supporting electrolyte. Because of poor solubility of the complex, a satisfied graph failed to be achieved in spite of several attempts. As depicted in Figure S1, the complex exhibits a less reversible oxidation wave at +1.28 V vs Ag/AgCl, which was assigned to metal-centered Ir^{IV}/Ir^{III} one-electron oxidation process according to the previous reports concerning analogous iridium complexes.[38,39] Also the complex showed a reversible reduction couple at −0.67 V, which is most likely assigned to the reduction of the coumarin 6 or dcbpy moiety.

Photoelectrochemical Property. The PEC property for $[(C6)_2Ir(dcbpy)]^+PF_6^-$ was investigated through covalently

DOI: 10.1021/acs.analchem.7b03229
Anal. Chem. 2017, 89, 11098–11106

attaching to the ITO electrode (Figure S2). The clean ITO was immersed in a mixture of H_2O, NH_4OH, and H_2O_2 (5:1:1, V/V/V) to introduce hydroxyl groups (−OH) on ITO surface. Then the ITO electrode was functionalized with NH_2 through the silanization using APTES as bifunctional linker. PEC active material, $[(C6)_2Ir(dcbpy)]^+PF_6^-$, was then covalently attached to the surface of ITO by virtue of amide bond.

Photocurrent action spectrum was acquired through changing the illumination wavelength over the range of 300−700 nm. As depicted in Figure S3, a maximum photocurrent peak appears at 475 nm, which is coincident with the maximum absorption peak of $[(C6)_2Ir(dcbpy)]^+PF_6^-$ (Figure 1), indicating that the generated photocurrent originate from the complex loaded on the ITO electrode.

A stable cathodic photocurrent (~1 $\mu A/cm^2$) was generated from $[(C6)_2Ir(dcbpy)]^+PF_6^-$ modified ITO electrode illuminated by a 475 nm light in 0.1 M PBS solution at 0 V bias voltage (pH = 7.4) (Figure 2A, curve c). The response was

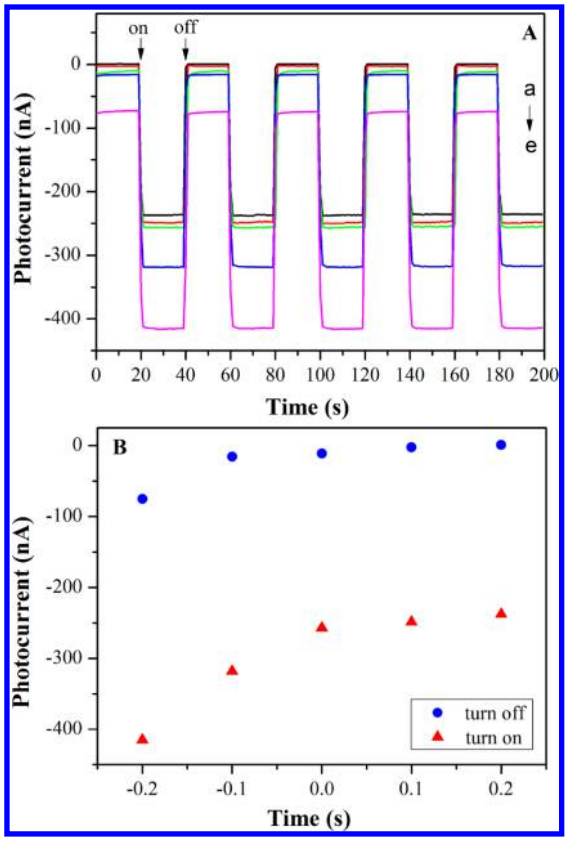

Figure 2. (A) Photocurrent changes induced by switching on and off the light (475 nm) illumination of the $[(C6)_2Ir(dcbpy)]^+PF_6^-$ attaching to the ITO electrode in 0.1 M PBS solution (pH = 7.4) at different bias voltage vs Ag/AgCl of (a) 0.2, (b) 0.1, (c) 0, (d) −0.1, (e) −0.2 V. (B) Effects of photocurrent intensities vs bias voltage based on panel A.

prompt and reproducible with negligible decay under 40 on−off cycles of illumination (Figure S4). The influences of applied bias voltage on photocurrent responses were investigated. As depicted in Figure 2, it is noteworthy that the negative bias voltages have a significant influence on the photocurrent intensity. And the stronger photocurrent was generated with the more negative bias voltage was applied, which may be due to increase of the charge transfer rate and inhibiting of the electron−hole pairs recombination.[40−42] A photocurrent density up to 1.8 $\mu A/cm^2$ at −0.2 V bias voltage was obtained. While positive bias voltages have an almost negligible influence on photocurrent. The dark current displays the same variation tendency to the photocurrent. The dark current from $[(C6)_2Ir(dcbpy)]^+PF_6^-$ is small or almost negligible when positive or 0 V bias voltage was applied. However, a great dark current was produced when negative bias voltage was applied, and up to 0.3 $\mu A/cm^2$ dark current was appeared at −0.2 V, which might originate from redox of Ir(III) complex according to similar characters of $Ru(bpy)_3^{2+}$ and Re(I) complex in previous reports.[41,43] The long-term stability of $[(C6)_2Ir(dcbpy)]^+PF_6^-$ modified ITO electrode was evaluated by measuring its photocurrent response every day over 7 days stored at 4 °C (Figure S5), the signal decay was negligible after 7 days, indicating good stability.

The maximum incident photon to current conversion efficiency (IPCE) was derived to be 0.47% according to the eq 1, which is more than the 0.38% of our previously reported $[(ppy)_2Ir(dppz)]^+PF_6^-$ and 0.065% of $[Ru(bpy)_2L](ClO_4)_2$ based multilayer film.

$$\mathrm{IPCE} = \frac{1240I\ (\mu A/cm^2)}{\lambda\ (nm)P_{inc}(W/m^2)} \quad (1)$$

where I is photocurrent intensity and P_{inc} is the incident light power. In this experiment, P_{inc} is 1000 W/m^2 and λ is 475 nm.

To elucidate the mechanisms responsible for cathodic photocurrent generation, the experiments were implemented in deaerated or air-equilibrated electrolyte solutions, respectively. As depicted in Figure S6, when the electrolyte solution was deaerated through bubbling N_2 for 15 min, the photocurrent decreased sharply by 60% at 0.1 V and 56% at 0 V, respectively, suggesting dissolved O_2 in the electrolyte solution played a vital role for cathodic photocurrent generation. To demonstrate the route of photocurrent generation, excited-state redox potentials of Ir(III) complex were estimated by means of UV−vis absorption spectra and cyclic voltammetry data. From an onset oxidation potential $E_{onset}(ox)$ at +1.12 V, the excited state redox potentials of $Ir^{IV}*/Ir^{III}$ was determined to be −1.13 V, according to the eq 2. The energy levels of the HOMO and LUMO for $[(C6)_2Ir(dcbpy)]^+PF_6^-$ were calculated to be −5.82 and −3.57 eV, respectively, by taking 4.7 eV for Ag/AgCl vs the vacuum level.

Employing estimated energy level values, the speculated cathodic photocurrent generation process is shown in Scheme 2. The process was initiated by the formation of the excited state $[(C6)_2Ir(dcbpy)]^{+}*$ because of the light illumination.

Scheme 2. Schematic Diagram of Electron Transfer Processes for Cathodic Photocurrent Generation from $[(C6)_2Ir(dcbpy)]^+PF_6^-$

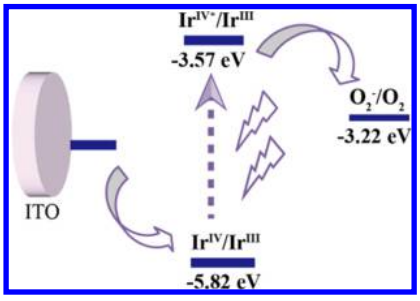

DOI: 10.1021/acs.analchem.7b03229
Anal. Chem. 2017, 89, 11098−11106

Scheme 3. Illustration of Exonuclease III-Assisted Recycling Amplification Strategy for PEC Detection of Thrombin: (A) Schematic Preparation Process of AuNPs Nanoprobes and (B) Schematic Process of Thrombin Recognition and Exonuclease III-Assisted Recycling Amplification

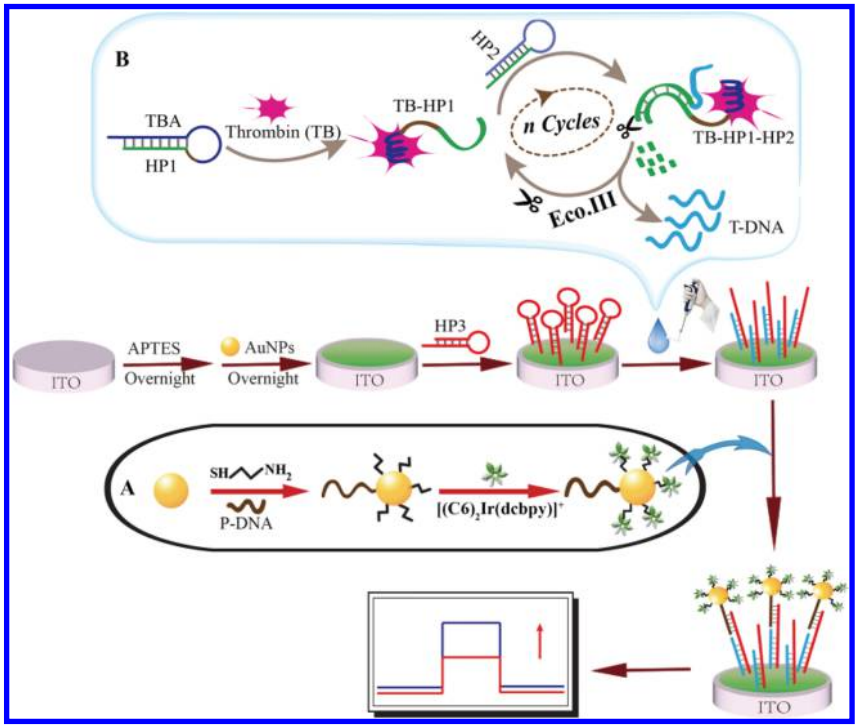

Subsequently, electron transfer from the excited state $[(C6)_2Ir(dcbpy)]^{+*}$ to the electron acceptor O_2 in the electrolyte solution. The conduction band of ITO electrode further donated an electron to regenerate the $[(C6)_2Ir(dcbpy)]^+$ ground state, triggering the photocurrent generation. The process of photocurrent generation can be described as eqs 3−5.

$$E(Ir^{IV*}/Ir^{III}) = E_{onset}(Ir^{IV*}/Ir^{III}) - E_{0-0} \quad (2)$$

$$[(C6)_2Ir(dcbpy)]^+ + h\upsilon \rightarrow [(C6)_2Ir(dcbpy)]^{+*} \quad (3)$$

$$[(C6)_2Ir(dcbpy)]^{+*} + O_2 \rightarrow [(C6)_2Ir(dcbpy)]^{2+} + O_2^- \quad (4)$$

$$[(C6)_2Ir(dcbpy)]^{2+} + e(CB) \rightarrow [(C6)_2Ir(dcbpy)]^+ \quad (5)$$

Preparation and Characterization of AuNPs-Based PEC Nanoprobe. Using as-prepared $[(C6)_2Ir(dcbpy)]^+PF_6^-$ as label, a PEC nanoprobe was constructed that relied on AuNPs to amplify signals and cysteamine as bifunctional linker, as depicted in Scheme 3. AuNPs was characterized by TEM and UV−vis absorption spectrum (Figure S7). The size of AuNPs was estimated with an average diameter of about 15 nm from the TEM images and absorption maximum at about 530 nm. As shown in Figure S8, the AuNPs-based nanoprobe exhibited combined characteristic absorbance features of the AuNPs (~530 nm) and Ir(III) complex (~480 nm), indicating the successful assembly of AuNPs and signal material $[(C6)_2Ir(dcbpy)]^+PF_6^-$.

Fabrication of the PEC Platform Based on Exonuclease III-Assisted Target Recycling Amplification. Bioactive molecules, such as nucleic acids, protein, and enzymes, play vital roles in various life processes and relates to a lot of diseases.[44−46] Unfortunately, its concentration is usually at a relatively low level in the early stage of diseases. Thus highly sensitive assays by virtue of signal amplification strategies are highly desirable to meet the demand for trace detection.[47−49] Exonuclease III (Exo III) could selectively catalyze the stepwise removal of mononucleotides from the blunt or recessed 3-hydroxyl termini of duplex DNAs.[50−52] Critically, it needs not a specific recognition site and shows limited activity on ssDNAs or protruding 3-termini of duplex DNAs. Recently, Exo III-assisted recycling means displayed great advantages for constructing amplified detection platforms.[53−57] Therefore, in this study, integrating Exo III-assisted signal amplification strategy with efficient iridium complex-based PEC nanoprobe, a strategy for bioanalysis was implemented with human thrombin as the model analyte, as shown in Scheme 3. In this assay, three hairpin probes (HP1, HP2, and HP3) with protruding 3′-terminus were involved in the amplification system, which existed stably in their respective stem-loop configuration in the absence of target protein. While in the presence of thrombin, the aptamer section of HP1 could bind to thrombin because of higher affinity, resulting in the conformation alteration of the HP1 and release of DNA fragment caged in the stem region, which subsequently hybridizes with HP2 to produce the double strands with a blunt 3′-terminus. Thus, Exo III cleavage process was triggered, accompanied with the following target recycling and autonomous release numerous secondary target fragment (T-DNA), which successively hybridized with the hairpin probe (HP3) on the electrode. Accordingly, signal nanoprobe was captured through hybridization of the released DNA fragment caged in HP3 with P-DNA attached to the AuNPs of nanoprobe, leading to a remarkable photocurrent response.

EIS Characterization of the PEC Platform Fabrication. The EIS was carried out to characterize the modified ITO electrode at different fabrication steps in the frequency range

DOI: 10.1021/acs.analchem.7b03229
Anal. Chem. 2017, 89, 11098−11106

from 0.1 Hz to 100 kHz and the results as Nyquist diagram are illustrated in Figure 3. The semicircle diameter at higher

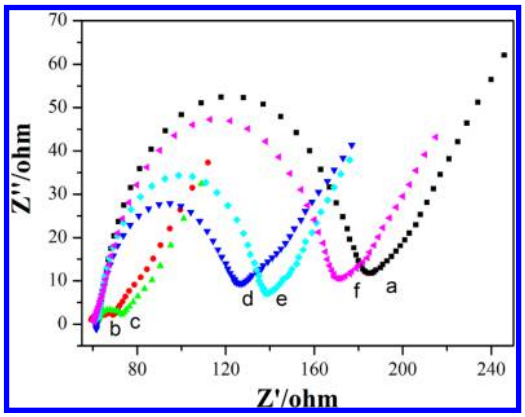

Figure 3. Electrochemical impedance spectroscopy of various electrodes assembly process (a) the bare ITO electrode, (b)ITO/APTES, (c) ITO/APTES/AuNPs, (d) ITO/APTES/AuNPs/HP3, (e) ITO/APTES/AuNPs/HP3/T-DNA, and (f) ITO/APTES/AuNPs/HP3/T-DNA/AuNPs probe. The spectra were recorded in 0.1 M pH 7.4 PBS including $Fe(CN_6)^{3-/4-}$ (10 mM) as the redox probe, applying a frequency of 100 kHz to 0.01 Hz under an amplitude of 5 mV.

frequencies signifies the electron transfer resistance (R_{et}), which represents the electron transfer process, while the linear part at lower frequencies means the diffusion process. The bare ITO electrode exhibited a large R_{et} value (curve a). R_{et} value decreased significantly (curve b) after self-assembling monolayer of APTES on the ITO electrode due to amino group, which might contribute to $Fe(CN_6)^{3-/4-}$ to diffuse onto the electrode surface. AuNPs assembled on the electrode surface did not obviously change the electron transfer resistance of the surface (curve c). Subsequently, immobilization of HP3 onto the modified ITO electrode caused an increase in R_{et} value (curve d) owing to the electrostatic repulsion between negative charges of the DNA and the $Fe(CN_6)^{3-/4-}$ redox probe. The R_{et} value was further increased when the modified electrode captured the released T-DNA fragment generated by Exo III-assisted target recycling process (curve e). When the AuNPs probes combined to the modified electrode, a largest R_{et} value (curve f) was observed. All the results indicate that the PEC platform was successful fabricated as expected.

Optimization of Experimental Conditions. To achieve the best performance of the PEC assay, the effects of the common electronic donor, TEOA, and AA, on the fabricated ITO electrode were investigated. The experiment results are depicted in Figure S9. When 0.1 M AA was added into the electrolyte solution, the photocurrent dramatically increased from 10 to 90 nA, indicating that AA is favorable in the electron-transfer process because of its strong reducibility. While adding the same concentration of TEOA to the electrolyte solution, no anticipated augment on photocurrent response were observed. To further acquire optimal operating conditions, the photocurrent dependence on the bias voltage using AA as electronic donor was also investigated. As shown in Figure 4, it could be found that photocurrent intensities increased with the augment of negative bias voltage applied to the electrode, which probably results from the same polarity for both. While positive bias voltage leads to the decrease of photocurrent intensities. Unfortunately, tremendous dark

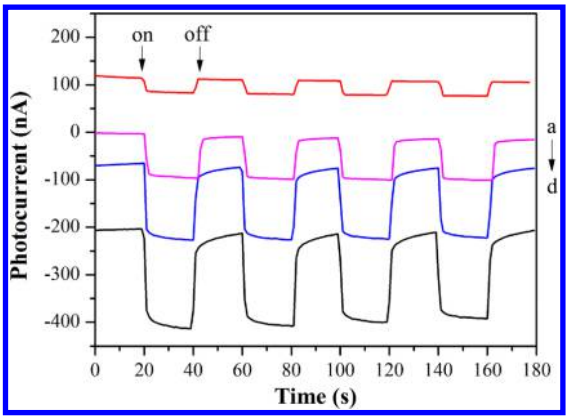

Figure 4. Effect of bias voltage on photocurrent response in 0.1 M PBS solution (pH = 7.4) at applied bias voltage of (a) +0.1, (b) 0, (c) −0.1, and (d) −0.2 V containing 0.1 MAA as sacrificial electron donor.

currents were generated when negative or positive bias voltages were applied. So 0 V of bias voltage is selected to the optimum condition in the following assays.

To explore the process of cathodic photocurrent generation employing AA as electronic donor, the experiments were performed in deaerated and air-equilibrated electrolyte solutions, respectively in the presence of AA. As depicted in Figure S10, no obvious change about the photocurrent response was seen when the electrolyte solution was deoxygenated, indicating dissolved O_2 in the electrolyte no longer be responsible for cathodic photocurrent generation. According to relevant reports,[58,59] the probable mechanism was speculated, as shown in Figure S11. The photocurrent generation route first involves the excited $[(C6)_2Ir(dcbpy)]^{+*}$ by photoexcitation. Then, the excited $[(C6)_2Ir(dcbpy)]^{+*}$ is reduced by AA to $[(C6)_2Ir(dcbpy)]$, in which the ligand C6 or dcbpy accepts an electron to L^- since Ir(III) cannot be electrochemically reduced.[60] The reduced $[(C6)_2Ir(dcbpy)]$ then reduce proton H^+ offered from AA to H_2. Thus $[(C6)_2Ir(dcbpy)]^+$ is regenerated and triggers the cathodic photocurrent generation.

In this assay, the PEC signal is highly dependent on the amount of nanoprobe captured on the electrode, which was significantly influenced by the hairpin probes concentration and amount of Exo III. To obtain the best performance of this PEC system, these experimental conditions were also optimized based on the photocurrent response toward 1 pM target thrombin. The HP1 probe concentration was first investigated since it has a significant effect to the amplification process. As shown in Figure S12A, the concentration of hairpin HP1 at 200 nM could obtain the optimum signal-to-background ratio (I/I_0). The higher concentration of hairpin probe could bounds each other to initiate the Exo III-catalyzed digestion, resulting in a relatively high background signal. The amount of Exo III is another key factor which has a crucial effect on the efficiency of the amplification. From Figure S12B, it can be found that the value of I/I_0 reach the maximum at the Exo III amount of 20 U. The decreased photocurrent intensity at more amount of Exo III could be due to a high background signal from the high cleavage activity of Exo III to HP1. The concentration of hairpin HP3 was also investigated since it influences the hybridization efficiency of P-DNA attached to Au nanoprobe. As depicted in Figure S12C, the value of I/I_0 increased with the increasing HP3 concentration, and reached the maximum at 1.0 μM, and then it tended to decrease. The decrease of

DOI: 10.1021/acs.analchem.7b03229
Anal. Chem. 2017, 89, 11098−11106

photocurrent response might be due to excess surface density of HP3 on electrode, leading to the increases of steric hindrance and the decrease of the hybridization efficiency. Thus 1.0 μM HP3 was chosen as the best assembly concentration in the following experiments.

Analytical Performance of the PEC Assay. On the basis of the strategy above, this PEC platform was served for thrombin detection. Under the optimized detection conditions, the performance of the constructed PEC platform was studied by varying the concentration of target thrombin. As depicted in Figure 5, a lower photocurrent was acquired in the absence of

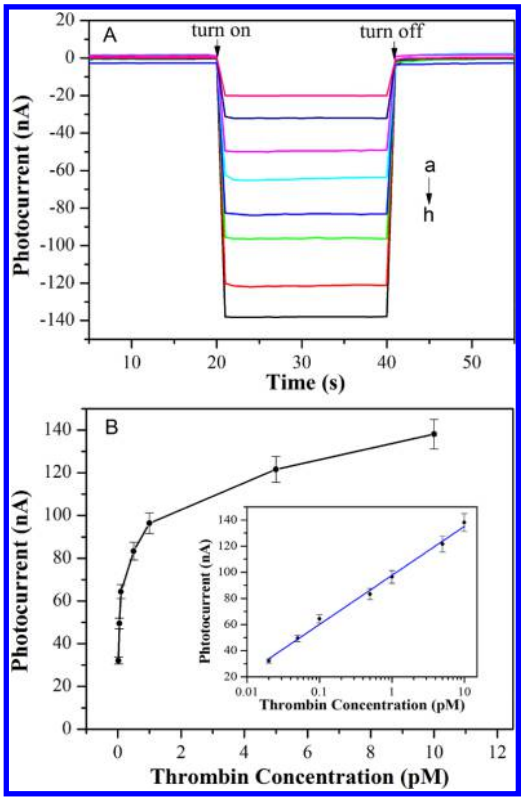

Figure 5. (A) Photocurrent responses of the PEC platform to different concentration of target thrombin (a) 0, (b) 20 fM, (c) 50 fM, (d) 100 fM, (e) 500 fM, (f) 1 pM, (g) 5 pM, and (h) 10 pM. Photocurrent measurement conditions. (B) The calibration curve of photocurrent (I) and logarithm of thrombin concentrations using the present platform. The error bars represent the standard deviation of three replicate assays.

thrombin. With the introduction of an increasing concentration of thrombin, the photocurrent gradually increased as expected, indicating that photocurrent response relied highly on the target concentration. The photocurrent intensity was logarithmically related to the thrombin concentrations across the range from 20 fM to 10 pM with a correlation coefficient of 0.9936 (Figure 5). The detection limit was estimated to be 9.6 fM at 3σ, suggesting prominent detection sensitivity compared with those of previously reported methods (Table S1). It is obvious that the improved sensitivity of this platform could be attributed to the admirable PEC nature of Ir(III) complex and efficient signal amplification strategy based on AuNPs and Exo III-assisted recycling. In addition, a relative standard deviation of 6.7% is obtained by detection thrombin at 100 fM with five repetitive measurements, indicating the fine reproducibility of the assay.

Selectivity of the Fabricated PEC Platform. The selectivity of the proposed strategy for thrombin detection was further evaluated by comparing the photocurrent responses toward BSA, IgG, and trypsin at the concentration of 1 pM. As shown in Figure 6, it can be seen that only the specific target

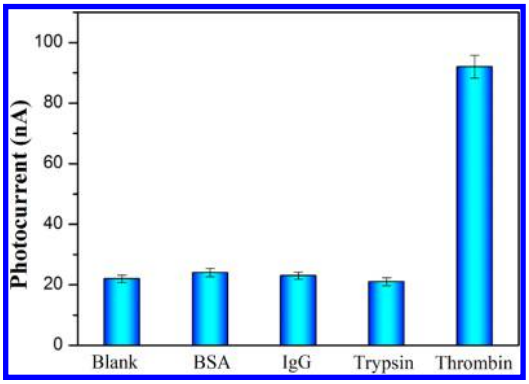

Figure 6. Selectivity investigation of the PEC platform for thrombin against other proteins including BSA, IgG, and trypsin. The employed proteins concentrations were all 1 pM. The error bars represented the standard deviation of three replicate determinations.

thrombin led to a remarkable photocurrent response, whereas photocurrent response was negligible compared to the control experiment in the presence of proteins of BSA, IgG, and trypsin. These results proved that the photocurrent response was specifically initiated by perfect binding of aptamer and target protein, indicating that the proposed PEC platform could provide a high specificity for protein assay.

Real Samples Analysis. The applicability of the proposed PEC assay in real samples was evaluated by the standard addition method. Three various concentrations of thrombin (50 fM, 500 fM, and 5 pM) were spiked into 20-fold diluted human serums. As listed in Table 1, the recoveries of three

Table 1. Determination of Thrombin in Human Serum Samples

sample	added (fM)	found (fM)[a]	recovery (%)	RSD (%)
1	50	51.3	102.6	5.6
2	500	493.5	98.7	4.1
3	5000	5215	104.3	6.4

[a]The content is the average of three independent experiments.

various thrombin concentrations were 102.6%, 98.7%, and 104.3%, respectively, and with the responding relative standard deviation of 5.6%, 4.1%, and 6.4%, demonstrating the feasibility of this proposed method in real biological samples with satisfactory results

CONCLUSIONS

In summary, a novel PEC active species, $[(C6)_2Ir(dcbpy)]^+PF_6^-$ employing coumarin 6 as a cyclometalated ligand, has been successfully synthesized and characterized. Significantly, the iridium(III) complex exhibits strong absorptions in the visible range with ε of more 40000 M^{-1} cm^{-1} at 480 nm. As evidenced by our research, the as-prepared Ir(III) complex exhibited a large cathodic photocurrent up to 1.8 μA/cm^2 using dissolved O_2 as electron acceptor irradiated by visible light. The AuNPs-based PEC nanoprobe has been constructed using $[(C6)_2Ir(dcbpy)]^+PF_6^-$ as signal reporter, and further

DOI: 10.1021/acs.analchem.7b03229
Anal. Chem. 2017, 89, 11098−11106

been applied to construct sensitive PEC platform based on the Exo III-assisted recycling amplification for thrombin detection. Ascribed to excellent PEC performance of the Ir(III) complex and the efficient amplifying strategy, a detection limit was achieved to be as low as 20 fM, which could rival or even exceed that of the reported excellent biosensors. To the best of our knowledge, this is the first study concerning visible-light induced Ir(III) complex for PEC active species. Our study would provide a promising avenue to develop visible-light harvesting Ir(III) complex photoactive material for PEC bioanalysis. It is expected that new family of Ir(III) complex possessing further red-shift the absorption in the visible and with increased IPCE to be designed for bioassay and clinical diagnoses.

■ ASSOCIATED CONTENT

Supporting Information

The Supporting Information is available free of charge on the ACS Publications website at DOI: 10.1021/acs.analchem.7b03229.

Preparation of the ligand C6 and the complex $[(C6)_2Ir(dcbpy)]^+PF_6^-$ preparation of AuNPs, cyclic voltammogram, photocurrent action spectrum, optimization of experimental conditions and comparison of various analytical methods for thrombin detection (PDF)

■ AUTHOR INFORMATION

Corresponding Author

*E-mail: tangb@sdnu.edu.cn. Fax: +86 53186180017.

ORCID

Bo Tang: 0000-0002-8712-7025

Author Contributions

The manuscript was written through contributions of all authors. All authors have given approval to the final version of the manuscript.

Notes

The authors declare no competing financial interest.

■ ACKNOWLEDGMENTS

This work was financially supported by the Natural Science Foundation of China (21775079, 21535004, and 21390411), Shandong Provincial Natural Science Foundation (ZR2017MB010), the Project of Shandong Province Higher Educational Science and Technology Program (J17KA106), and the State Key Laboratory of Analytical Chemistry for Life Science (SKLACLS1503).

■ REFERENCES

(1) Zhao, W. W.; Xu, J. J.; Chen, H. Y. *Chem. Rev.* **2014**, *114*, 7421−7441.
(2) Zhao, W. W.; Xu, J. J.; Chen, H. Y. *Chem. Soc. Rev.* **2015**, *44*, 729−741.
(3) Li, R.; Zhang, Y.; Tu, W.; Dai, Z. *ACS Appl. Mater. Interfaces* **2017**, *9*, 22289−22297.
(4) Zhao, W. W.; Yu, P. P.; Shan, Y.; Wang, J.; Xu, J. J.; Chen, H. Y. *Anal. Chem.* **2012**, *84*, 5892−5897.
(5) Wen, G.; Ju, H. *Anal. Chem.* **2016**, *88*, 8339−8345.
(6) Zhao, M.; Fan, G. C.; Chen, J. J.; Shi, J. J.; Zhu, J. J. *Anal. Chem.* **2015**, *87*, 12340−12347.
(7) Fan, G.-C.; Zhao, M.; Zhu, H.; Shi, J.-J.; Zhang, J.-R.; Zhu, J.-J. *J. Phys. Chem. C* **2016**, *120*, 15657−15665.
(8) Hou, T.; Zhang, L.; Sun, X.; Li, F. *Biosens. Bioelectron.* **2016**, *75*, 359−364.
(9) Bünzli, J.-C. G. *Chem. Rev.* **2010**, *110*, 2729−2755.
(10) Liang, M.; Liu, S.; Wei, M.; Guo, L. H. *Anal. Chem.* **2006**, *78*, 621−623.
(11) Liang, M.; Jia, S.; Zhu, S.; Guo, L.-H. *Environ. Sci. Technol.* **2008**, *42*, 635−639.
(12) Dong, D.; Zheng, D.; Wang, F. Q.; Yang, X. Q.; Wang, N.; Li, Y. G.; Guo, L. H.; Cheng, J. *Anal. Chem.* **2004**, *76*, 499−501.
(13) Zhang, X.; Guo, Y.; Liu, M.; Zhang, S. *RSC Adv.* **2013**, *3*, 2846−2857.
(14) Lo, S.-C.; Harding, R. E.; Shipley, C. P.; Stevenson, S. G.; Burn, P. L.; Samuel, I. D. *J. Am. Chem. Soc.* **2009**, *131*, 16681−16688.
(15) Graber, S.; Doyle, K.; Neuburger, M.; Housecroft, C. E.; Constable, E. C.; Costa, R. D.; Orti, E.; Repetto, D.; Bolink, H. J. *J. Am. Chem. Soc.* **2008**, *130*, 14944−14945.
(16) Huang, J.; Yu, J.; Guan, Z.; Jiang, Y. *Appl. Phys. Lett.* **2010**, *97*, 143301.
(17) Xu, Z.; Hu, B.; Howe, J. *J. Appl. Phys.* **2008**, *103*, 043909.
(18) You, Y.; Nam, W. *Chem. Soc. Rev.* **2012**, *41*, 7061−7084.
(19) Goldsmith, J. I.; Hudson, W. R.; Lowry, M. S.; Anderson, T. H.; Bernhard, S. *J. Am. Chem. Soc.* **2005**, *127*, 7502−7510.
(20) Jasimuddin, S.; Yamada, T.; Fukuju, K.; Otsuki, J.; Sakai, K. *Chem. Commun.* **2010**, *46*, 8466−8468.
(21) Baranoff, E.; Yum, J.-H.; Graetzel, M.; Nazeeruddin, M. K. *J. Organomet. Chem.* **2009**, *694*, 2661−2670.
(22) Mayo, E. I.; Kilså, K.; Tirrell, T.; Djurovich, P. I.; Tamayo, A.; Thompson, M. E.; Lewis, N. S.; Gray, H. B. *Photochem. Photobiol. Sci.* **2006**, *5*, 871−873.
(23) You, Y.; Park, S. Y. *Dalton Trans.* **2009**, *8*, 1267−1282.
(24) Le Goff, A.; Cosnier, S. *J. Mater. Chem.* **2011**, *21*, 3910−3915.
(25) Li, C.; Wang, H.; Shen, J.; Tang, B. *Anal. Chem.* **2015**, *87*, 4283−4291.
(26) Lo, K. K.-W.; Li, S. P.-Y.; Zhang, K. Y. *New J. Chem.* **2011**, *35*, 265−287.
(27) Zhao, J.; Wu, W.; Sun, J.; Guo, S. *Chem. Soc. Rev.* **2013**, *42*, 5323−5351.
(28) Lamansky, S.; Djurovich, P.; Murphy, D.; Abdel-Razzaq, F.; Lee, H.-E.; Adachi, C.; Burrows, P. E.; Forrest, S. R.; Thompson, M. E. *J. Am. Chem. Soc.* **2001**, *123*, 4304−4312.
(29) Takizawa, S. Y.; Ikuta, N.; Zeng, F.; Komaru, S.; Sebata, S.; Murata, S. *Inorg. Chem.* **2016**, *55*, 8723−8735.
(30) Sinopoli, A.; Wood, C. J.; Gibson, E. A.; Elliott, P. I. *Eur. J. Inorg. Chem.* **2016**, *2016*, 2887−2890.
(31) Chao, R. Y.; Ding, M. F.; Chen, J. Y.; Lee, C. C.; Lin, S. T. *J. Chin. Chem. Soc.* **2010**, *57*, 213−221.
(32) Luo, X.; Song, J.; Cheng, L.; Huang, D. *Sci. China, Ser. B: Chem.* **2001**, *44*, 532−539.
(33) Nonoyama, M. *Bull. Chem. Soc. Jpn.* **1974**, *47*, 767−768.
(34) Grabar, K. C.; Smith, P. C.; Musick, M. D.; Davis, J. A.; Walter, D. G.; Jackson, M. A.; Guthrie, A. P.; Natan, M. J. *J. Am. Chem. Soc.* **1996**, *118*, 1148−1153.
(35) Duan, R.; Zhou, X.; Xing, D. *Anal. Chem.* **2010**, *82*, 3099−3103.
(36) Tamayo, A. B.; Alleyne, B. D.; Djurovich, P. I.; Lamansky, S.; Tsyba, I.; Ho, N. N.; Bau, R.; Thompson, M. E. *J. Am. Chem. Soc.* **2003**, *125*, 7377−7387.
(37) Laskar, I. R.; Chen, T.-M. *Chem. Mater.* **2004**, *16*, 111−117.
(38) Lo, K. K.-W.; Chung, C.-K.; Lee, T. K.-M.; Lui, L.-H.; Tsang, K. H.-K.; Zhu, N. *Inorg. Chem.* **2003**, *42*, 6886−6897.
(39) Avilov, I.; Minoofar, P.; Cornil, J.; De Cola, L. *J. Am. Chem. Soc.* **2007**, *129*, 8247−8258.
(40) Jiang, K.; Xie, H.; Zhan, W. *Langmuir* **2009**, *25*, 11129−11136.
(41) Meng, T. T.; Zheng, Z. B.; Wang, K. Z. *Langmuir* **2013**, *29*, 14314−14320.
(42) Wu, D.-G.; Huang, C.-H.; Gan, L.-B.; Zheng, J.; Huang, Y.-Y.; Zhang, W. *Langmuir* **1999**, *15*, 7276−7281.
(43) Ju, C.-C.; Zhang, A.-G.; Sun, H.-L.; Wang, K.-Z.; Jiang, W.-L.; Bian, Z.-Q.; Huang, C.-H. *Organometallics* **2011**, *30*, 712−716.

DOI: 10.1021/acs.analchem.7b03229
Anal. Chem. 2017, 89, 11098−11106

(44) Dexheimer, T. S.; Sun, D.; Hurley, L. H. *J. Am. Chem. Soc.* **2006**, *128*, 5404−5415.
(45) Kulasingam, V.; Diamandis, E. P. *Nat. Clin. Pract. Oncol.* **2008**, *5*, 588−599.
(46) Wood, S. L.; Knowles, M. A.; Thompson, D.; Selby, P. J.; Banks, R. E. *Nat. Rev. Urol.* **2013**, *10*, 206−218.
(47) Turner, A. P. *Chem. Soc. Rev.* **2013**, *42*, 3184−3196.
(48) Liu, J.; Cao, Z.; Lu, Y. *Chem. Rev.* **2009**, *109*, 1948−1998.
(49) Ge, L.; Wang, W.; Hou, T.; Li, F. *Biosens. Bioelectron.* **2016**, *77*, 220−226.
(50) Richardson, C. C.; Lehman, I.; Kornberg, A. *J. Biol. Chem.* **1964**, *239*, 251−258.
(51) Wang, J.; Li, T.; Guo, X.; Lu, Z. *Nucleic Acids Res.* **2005**, *33*, e23−e23.
(52) Kurita, H.; Inaishi, K.-i.; Torii, K.; Urisu, M.; Nakano, M.; Katsura, S.; Mizuno, A. *J. Biomol. Struct. Dyn.* **2008**, *25*, 473−480.
(53) Gao, Y.; Li, B. *Anal. Chem.* **2014**, *86*, 8881−8887.
(54) Li, Y.; Zhao, Q.; Wang, Y.; Man, T.; Zhou, L.; Fang, X.; Pei, H.; Chi, L.; Liu, J. *Anal. Chem.* **2016**, *88*, 11684−11690.
(55) Wang, X.; Hou, T.; Lu, T.; Li, F. *Anal. Chem.* **2014**, *86*, 9626−9631.
(56) Xiong, E.; Yan, X.; Zhang, X.; Liu, Y.; Zhou, J.; Chen, J. *Biosens. Bioelectron.* **2017**, *87*, 732−736.
(57) Xiong, E.; Zhang, X.; Liu, Y.; Zhou, J.; Yu, P.; Li, X.; Chen, J. *Anal. Chem.* **2015**, *87*, 7291−7296.
(58) Zeng, X.; Ma, S.; Bao, J.; Tu, W.; Dai, Z. *Anal. Chem.* **2013**, *85*, 11720−11724.
(59) Wang, F.; Wang, W. G.; Wang, X. J.; Wang, H. Y.; Tung, C. H.; Wu, L. Z. *Angew. Chem., Int. Ed.* **2011**, *50*, 3193−3197.
(60) Palmer, J. H.; Wilson, A. D.; Henling, L. M.; Gross, Z.; Gray, H. B.; et al. *J. Am. Chem. Soc.* **2008**, *130*, 7786−7787.

DOI: 10.1021/acs.analchem.7b03229
Anal. Chem. 2017, 89, 11098−11106